Chin. Ann. Math.
30B(5), 2009, 447–462
DOI: 10.1007/s11401-009-0088-3

Chinese Annals of Mathematics, Series B

Short-Time Linear Response with Reduced-Rank Tangent Map**

Rafail V. ABRAMOV*

(*Dedicated to Professor Andrew Majda on the Occasion of his* 60*th Birthday*)

Abstract The recently developed short-time linear response algorithm, which predicts the response of a nonlinear chaotic forced-dissipative system to small external perturbation, yields high precision of the response prediction. However, the computation of the short-time linear response formula with the full rank tangent map can be expensive. Here, a numerical method to potentially overcome the increasing numerical complexity for large scale models with many variables by using the reduced-rank tangent map in the computation is proposed. The conditions for which the short-time linear response approximation with the reduced-rank tangent map is valid are established, and two practical situations are examined, where the response to small external perturbations is predicted for nonlinear chaotic forced-dissipative systems with different dynamical properties.

Keywords Fluctuation-dissipation theorem, Linear response
2000 MR Subject Classification 65, 82, 86

1 Introduction

The fluctuation-dissipation theorem (FDT) is one of the cornerstones of modern statistical physics, discovered about eighty years ago. Roughly speaking, the fluctuation-dissipation theorem states that, for dynamical systems at statistical equilibrium, the average response to small external perturbations can be calculated through the knowledge of suitable correlation functions of the unperturbed dynamical system. The fluctuation-dissipation theorem has great practical use in traditional setting involving statistical equilibrium of baths of identical gas or liquid molecules, Ornstein-Uhlenbeck Brownian motion, motion of electric charges, turbulence, quantum field theory, chemical physics, physical chemistry and other areas. The general advantage provided by the fluctuation-dissipation theorem is that one can successfully predict the response of a dynamical system at statistical equilibrium to an arbitrary small external perturbation without ever observing the behavior of the perturbed system, which offers great versatility and insight in understanding the behavior of dynamical processes near equilibrium in numerous scientific applications (see [10, 18]).

Manuscript received March 24, 2009. Published online August 10, 2009.
*Department of Mathematics, Statistics and Computer Science, University of Illinois at Chicago, 1223 SEO, 851 S. Morgan St., IL 60607, Chicago, USA. E-mail: abramov@math.uic.edu
**Project supported by the National Science Foundation (No. DMS-0608984) and the Office of Naval Research (No. N00014-06-1-0286).

Despite the facts that the climate system is a complex chaotic multiscale problem with forcing and dissipation and that the equilibrium state structure has significant complexity, there has been a profound interest among the atmospheric/ocean science community to apply the fluctuation-dissipation theorem to predict global climate changes responding to variation of certain physical parameters (see [5–7, 13–17, 19, 22]), where the FDT has been used largely in its classical formulation (see [23]).

However, the fluctuation-dissipation theorem in its classical formulation is only partially successful for nonlinear dynamical systems with forcing and dissipation. The major difficulty in this situation is that the probability measure in the limit as time approaches infinity in this case is typically a Sinai-Ruelle-Bowen probability measure, which is supported on a large-dimensional (often fractal) set and is usually not absolutely continuous with respect to the Lebesgue measure (see [9, 27]). In the context of Axiom A attractors, Ruelle [24, 25] has adapted the classical calculations for FDT to this setting. In this context, Majda and the author [1–3] developed and tested a novel computational algorithm for predicting the mean response of functionals of a chaotic dynamical system to small change in external forcing via the fluctuation-dissipation theorem. This algorithm, called the short-time FDT (ST-FDT) algorithm in [1–3], takes into account the fact that the dynamics of chaotic nonlinear forced-dissipative systems often reside on chaotic fractal attractors, where the classical quasi-Gaussian formula of the fluctuation-dissipation theorem often fails to produce satisfactory response prediction, especially in dynamical regimes with weak and moderate chaos and slower mixing. It has been discovered in [1–3] that the ST-FDT algorithm is an extremely precise response approximation for short response times, but numerically unstable for longer response times.

However, the computation of the short-time linear response formula from [1–3] with the full rank tangent map is numerically expensive. Here we propose a numerical method to potentially overcome the increasing numerical complexity for large scale models with many variables by using the reduced-rank tangent map in the computation of the linear response. We establish the conditions for which the short-time linear response approximation with the reduced-rank tangent map is valid, and examine two practical situations, where the linear response is predicted for nonlinear chaotic forced-dissipative systems with different properties.

2 Short-Time Linear Response Formula

Here we start with the derivation of the fluctuation-dissipation theorem in its geometric formulation, following Ruelle [25]. A dynamical system of chaotic ODEs for a vector $\vec{x} \in \mathbb{R}^N$ is given by

$$\dot{\vec{x}}(t) = \vec{f}(\vec{x}(t)), \quad \vec{x}(t) = \phi^t \vec{x}, \tag{2.1}$$

where $\vec{f}$ is a differentiable vector field of dimension N, and ϕ^t is the flow generated by $\vec{f}$. We also assume that, for a suitable large set of initial conditions, there is an ergodic invariant probability measure $\rho_{\vec{f}}$ such that, for any smooth function $A(\vec{x})$ and for any t,

$$\rho_{\vec{f}}(A) = \rho_{\vec{f}}(A \circ \phi^t), \tag{2.2}$$

where

$$\rho_{\vec{f}}(A) = \int A(\vec{x}) \rho_{\vec{f}}(\mathrm{d}\vec{x}). \tag{2.3}$$

Now, let a small forcing be introduced into the right-hand side of (2.1):

$$\dot{\vec{x}}(t) = \vec{f}(\vec{x}(t)) + w(\vec{x}(t))\delta\vec{f}(t), \quad \vec{x}(t) = \widehat{\phi}^t\vec{x}, \tag{2.4}$$

where $w(\vec{x})$ is an $N \times K$ matrix, $\delta\vec{f}(t)$ is a small K-dimensional time-dependent forcing such that $\delta\vec{f}(t) = 0$ when $t < 0$, and $\widehat{\phi}^t$ is the flow operator generated by the right-hand side of (2.4). Then the response $\delta_t\rho_{\vec{f}}(A)$ of $\rho_{\vec{f}}(A)$ to the small perturbation in the right-hand side of (2.4) is defined by

$$\delta_t\rho_{\vec{f}}(A) = \rho_{\vec{f}}(A \circ \widehat{\phi}^t - A \circ \phi^t). \tag{2.5}$$

At this point, we are going to derive a suitable approximation of the response $\delta_t\rho_{\vec{f}}(A)$ in (2.5), which is linear with respect to the small perturbation $\delta\vec{f}(t)$.

Formally expanding (2.5) with respect to $\delta\phi^t\vec{x} = \widehat{\phi}^t\vec{x} - \phi^t\vec{x}$ and discarding higher order terms, we obtain

$$\delta_t\rho_{\vec{f}}(A) = \int \nabla A(\phi^t\vec{x})\delta\phi^t\vec{x}\rho_{\vec{f}}(\mathrm{d}\vec{x}). \tag{2.6}$$

The linear approximation in (2.6) necessitates a suitable linear approximation for $\delta\phi^t\vec{x}$. Subtracting (2.1) from (2.4), expanding with respect to $\delta\phi^t\vec{x}$ and discarding higher order terms, we find

$$\frac{\partial}{\partial t}\delta\phi^t\vec{x} = J(\phi^t\vec{x})\delta\phi^t\vec{x} + w(\phi^t\vec{x})\delta\vec{f}(t), \quad \delta\phi^0\vec{x} = 0, \tag{2.7}$$

where

$$J(\vec{x}) = \frac{\partial\vec{f}}{\partial\vec{x}}$$

is the Jacobian of the vector field $\vec{f}$. The formal solution to this linear equation is given by the Duhamel's principle:

$$\delta\phi^t\vec{x} = \int_0^t \mathrm{e}^{\int_\tau^t J(\phi^s\vec{x})\mathrm{d}s} w(\phi^\tau\vec{x})\delta\vec{f}(\tau)\mathrm{d}\tau. \tag{2.8}$$

In order to interpret the semigroup notation above in (2.8), we differentiate (2.1) with respect to $\vec{x}$:

$$\frac{\partial}{\partial t}\Big(\frac{\partial\phi^t\vec{x}}{\partial\vec{x}}\Big) = \vec{J}(\phi^t\vec{x})\frac{\partial\phi^t\vec{x}}{\partial\vec{x}}. \tag{2.9}$$

Defining the tangent map as $T^t_{\vec{x}} = \frac{\partial\phi^t\vec{x}}{\partial\vec{x}}$, we obtain

$$\dot{T}^t_{\vec{x}} = \vec{J}(\phi^t\vec{x})T^t_{\vec{x}}. \tag{2.10}$$

Since $\phi^t = \phi^{t-\tau} \circ \phi^\tau$ for an arbitrary τ, the chain rule of differentiation yields $T^t_{\vec{x}} = T^{t-\tau}_{\phi^\tau\vec{x}}T^\tau_{\vec{x}}$. Substituting the chain rule into (2.10) and multiplying both sides by $T^{-\tau}_{\phi^\tau\vec{x}}$, we obtain

$$\dot{T}^{t-\tau}_{\phi^\tau\vec{x}} = J(\phi^t\vec{x})T^{t-\tau}_{\phi^\tau\vec{x}}, \quad \forall\,\vec{x}, t, \tau, \tag{2.11}$$

with the formal solution

$$T^{t-\tau}_{\phi^\tau\vec{x}} = \mathrm{e}^{\int_\tau^t J(\phi^s\vec{x})\mathrm{d}s}. \tag{2.12}$$

The latter yields

$$\delta\phi^t\vec{x} = \int_0^t T^{t-\tau}_{\phi^\tau\vec{x}} w(\phi^\tau\vec{x})\delta\vec{f}(\tau)\mathrm{d}\tau. \tag{2.13}$$

Substituting (2.13) into (2.6), one obtains

$$\begin{aligned}\delta_t\rho_{\vec{f}}(A) &= \int_0^t \Big[\int \nabla A(\phi^t\vec{x})T^{t-\tau}_{\phi^\tau\vec{x}}w(\phi^\tau\vec{x})\rho_{\vec{f}}(\mathrm{d}\vec{x})\Big]\delta\vec{f}(\tau)\mathrm{d}\tau \\ &= \int_0^t \Big[\int \nabla A(\phi^{t-\tau}\vec{x})T^{t-\tau}_{\vec{x}}w(\vec{x})\rho_{\vec{f}}(\mathrm{d}\vec{x})\Big]\delta\vec{f}(\tau)\mathrm{d}\tau, \end{aligned} \tag{2.14}$$

where for the second equality we used the fact that $\rho_{\vec{f}}$ is an invariant probability measure for ϕ^t. Finally, one can write the linear fluctuation-dissipation formula as

$$\begin{aligned}\delta_t\rho_{\vec{f}}(A) &= \int_0^t R(t-\tau)\delta\vec{f}(\tau), \\ R(t) &= \int \nabla A(\phi^t\vec{x})T^t_{\vec{x}}w(\vec{x})\rho_{\vec{f}}(\mathrm{d}\vec{x}).\end{aligned} \tag{2.15}$$

Using ergodicity of $\rho_{\vec{f}}$ and replacing space averages with time averages, one can write the kernel of the linear response operator $R(t)$ as

$$R(t) = \lim_{s\to\infty}\frac{1}{s}\int_0^s \nabla A(\vec{x}(t+\tau))T^t_{\vec{x}(\tau)}w(\vec{x}(\tau))\mathrm{d}\tau. \tag{2.16}$$

It has to be mentioned that if the probability measure $\rho_{\vec{f}}$ is absolutely continuous with respect to the Lebesgue's measure $\mathrm{d}\vec{x}$, i.e., $\rho_{\vec{f}}(\mathrm{d}\vec{x}) = p(\vec{x})\mathrm{d}\vec{x}$ with $p(\vec{x})$ being smooth probability density function, then one can integrate the second formula in (2.15) by parts, obtaining

$$R(t) = -\int A(\phi^t\vec{x})\mathrm{div}(w(\vec{x})p(\vec{x}))\mathrm{d}\vec{x}. \tag{2.17}$$

In particular, replacing space average with time average above yields the classical fluctuation-dissipation formula:

$$R(t) = -\lim_{s\to\infty}\frac{1}{s}\int_0^s A(\vec{x}(t+\tau))[\mathrm{div}w + w\nabla\ln p](\vec{x}(\tau))\mathrm{d}\tau. \tag{2.18}$$

2.1 Short time linear response formula for nonlinear maps

In practice, the dynamical system of the form (2.1) typically cannot be explicitly solved. Common methods of solution involve discretization in time, when continuous time variable t is replaced with a set discretized time steps $n\Delta t$. For a single-step explicit time integration scheme (such as, for instance, the standard 4th order Runge-Kutta method) and $\vec{x}\in\mathbb{R}^N$, the dynamical system in (2.1) assumes the form of a nonlinear map

$$\vec{x}_{n+1} = \vec{F}(\vec{x}_n), \tag{2.19}$$

where $\vec{F}$ is a vector-valued nonlinear function provided by the vector field $\vec{f}$ and the chosen time integration scheme. Here we omit the discrete time parameter Δt for convenience.

Here we assume that, just like for continuous dynamical systems above, for a large set of initial conditions the nonlinear map $\vec{F}$ has an ergodic invariant probability measure $\rho_{\vec{F}}$ such that for any observable $A(\vec{x})$ and any integer k,

$$\rho_{\vec{F}}(A) = \rho_{\vec{F}}(A\circ\vec{F}^k). \tag{2.20}$$

Now, assume that a small forcing is introduced into the right-hand side of (2.19):

$$\vec{x}_{n+1} = \vec{\tilde{F}}(\vec{x}_n) = \vec{F}(\vec{x}_n) + w(\vec{x}_n)\delta\vec{F}_n, \tag{2.21}$$

where $w(\vec{x})$ is an $N \times K$ matrix, and $\delta\vec{F}_n$ is a small K-dimensional time-dependent forcing. Then the response of A is defined by

$$\delta_k \rho_{\vec{F}}(A) = \rho_{\vec{F}}(A \circ \vec{\tilde{F}} - A \circ \vec{F}). \tag{2.22}$$

Formally expanding (2.22) with respect to $\delta\vec{x}_k = \vec{\tilde{F}}^k(\vec{x}_0) - \vec{F}^k(\vec{x}_0)$ and discarding higher order terms, we obtain

$$\delta_k \rho_{\vec{F}}(A) = \int \nabla A(\vec{F}^k(\vec{x}))\delta\vec{x}_k \rho_{\vec{F}}(\mathrm{d}\vec{x}). \tag{2.23}$$

Now one needs to find a suitable linear approximation for $\delta\vec{x}_k$. Subtracting (2.19) from (2.21), expanding with respect to $\delta\vec{x}$ and discarding higher order terms, we find

$$\delta\vec{x}_{n+1} = T(\vec{x}_n)\delta\vec{x}_n + w(\vec{x}_n)\delta\vec{F}_n, \tag{2.24}$$

where $T(\vec{x}_n)$ is the one-step tangent map of $\vec{F}(\vec{x}_n)$ (Jacobian matrix of $\vec{F}(\vec{x}_n)$). Due to the linearity of (2.24), one finds

$$\delta\vec{x}_n = \sum_{k=0}^{n-1} T^{n-k-1}_{\vec{x}_{k+1}} w(\vec{x}_k)\delta F_k, \tag{2.25}$$

where the m-step tangent map is given by the product of the one-step tangent maps:

$$T^m_{\vec{x}_n} = \prod_{k=0}^{m-1} T(\vec{x}_{n+k}). \tag{2.26}$$

Substituting (2.25) into (2.23), one obtains

$$\begin{aligned}\delta_n \rho_{\vec{F}}(A) &= \sum_{k=0}^{n-1} \Big[\int \nabla A(\vec{F}^n(\vec{x})) T^{n-k-1}_{\vec{F}^{k+1}(\vec{x})} w(\vec{F}^k(\vec{x}))\rho_{\vec{F}}(\mathrm{d}\vec{x}) \Big] \delta\vec{F}_k \\ &= \sum_{k=0}^{n-1} \Big[\int \nabla A(\vec{F}^{n-k}(\vec{x})) T^{n-k-1}_{\vec{F}(\vec{x})} w(\vec{x})\rho_{\vec{F}}(\mathrm{d}\vec{x}) \Big] \delta\vec{F}_k, \end{aligned} \tag{2.27}$$

where for the second equality we used the fact that $\rho_{\vec{F}}$ is an invariant probability measure for $\vec{F}$. Finally, one can write the linear fluctuation-dissipation formula as

$$\begin{aligned}\delta_n \rho_{\vec{F}}(A) &= \sum_{k=0}^{n-1} R_{n-k}\delta\vec{F}_k, \\ R_m &= \int \nabla A(\vec{F}^m(\vec{x})) T^{m-1}_{\vec{F}(\vec{x})} w(\vec{x})\rho_{\vec{F}}(\mathrm{d}\vec{x}). \end{aligned} \tag{2.28}$$

Using ergodicity of $\rho_{\vec{F}}$ and replacing space averages with time averages, one can write the linear response operator R_m as

$$R_m = \lim_{k\to\infty} \frac{1}{k} \sum_{n=1}^{k} \nabla A(\vec{x}_{m+n}) T^{m-1}_{\vec{x}_{n+1}} w(\vec{x}_n). \tag{2.29}$$

For chaotic maps, the computation of R_m above becomes numerically unstable for large m, due to the fact that some entries of the multistep tangent map $T^m_{\vec{x}_n}$ grow exponentially fast with increasing m.

3 The Algorithm for the Reduced-Rank Tangent Map

Here we start with a description of the existing computational algorithm for the tangent map $T^m_{\vec{x}_n}$, which is used in [1–3]. While the formula in (2.26) is sufficient to compute the discretized version of the tangent maps for different number of steps m, in practice a more advanced approach is taken. For each $N \times N$ single-step tangent map $T(\vec{x}_k)$ we perform the following recursive QR-decomposition:

$$[T(\vec{x}_k)Q_k] = Q_{k+1}R_{k+1}, \tag{3.1}$$

where Q_k is an $N \times N$ orthogonal matrix, and R_k is an $N \times N$ upper-triangular matrix with nonnegative diagonal entries. The initial matrix Q_0 is an arbitrary $N \times N$ orthogonal matrix, and for practical purposes Q_0 can be set to identity.

The QR-decomposition in (3.1) yields the following formula for the m-step tangent map in (2.26):

$$T^m_{\vec{x}_n} = Q_{m+n}R_{m+n} \cdots R_{n+1}Q_n^T. \tag{3.2}$$

At first, it seems that the simple formula in (2.26) requires less computational effort than the two formulas in (3.1) and (3.2), which is indeed true for the computation of a single m-step tangent map. However, in order to compute the short-time linear response operator in (2.29) for a fixed m as a time-average over n, m-fold matrix products either in (2.26) or in (3.2) have to be computed for every step n, while the QR-decomposition in (3.1) has to be computed only once per time step n irrespective of m. Due to the fact that R_k are upper-triangular matrices, for large m the computation of (3.2) is faster than that of (2.26) by a factor of 6.

However, the computation of the tangent map in (3.2) is numerically expensive. In the majority of practical applications the nonlinearity in $\vec{f}$ from (2.1) is quadratic, which typically yields $O(N^2)$ numerical complexity in (2.19), or even better. On the other hand, the numerical complexity of (3.2) is $O(N^3)$, and for many degrees of freedom ($N \sim$ several hundred) the computation of (3.2) becomes overwhelming.

Here we propose a numerical method to potentially overcome increasing numerical complexity in (3.2) by using a reduced number of columns in Q_k. In general, for an arbitrary $N \times L$ matrix, $N \geq L$, the QR-decomposition yields the $N \times L$ orthogonal matrix Q and the $L \times L$ upper-triangular matrix R. The algorithm is defined as follows:

(1) Choose $1 \leq L \leq N$.

(2) For each single-step tangent map $T(\vec{x}_k)$, perform the QR-decomposition:

$$[T(\vec{x}_k)\widetilde{Q}_k] = \widetilde{Q}_{k+1}\widetilde{R}_{k+1}, \tag{3.3}$$

where $\widetilde{Q}_0$ is an arbitrary $N \times L$ orthogonal matrix. Then $[T(\vec{x}_k)\widetilde{Q}_{k-1}]$ is an $N \times L$ matrix and, therefore, $\widetilde{Q}_k$ and $\widetilde{R}_k$ are $N \times L$ orthogonal and $L \times L$ upper-triangular matrices, respectively.

(3) The formula for the reduced-rank tangent map is

$$\widetilde{T}^m_{\vec{x}_n} = \widetilde{Q}_{m+n}\widetilde{R}_{m+n} \cdots \widetilde{R}_{n+1}\widetilde{Q}_n^T. \tag{3.4}$$

It is easy to see that $\widetilde{T}^m_{\vec{x}_n}$ is still an $N \times N$ matrix just like the original tangent map $T^m_{\vec{x}_n}$, but $\widetilde{T}^m_{\vec{x}_n}$ has rank L. The computational complexity of (3.4) is $O(L^3)$, rather than $O(N^3)$.

Of course, for the reduced-rank tangent map $\widetilde{T}^m_{\vec{x}_n}$, one can expect increased numerical errors in the linear response formula in (2.29), if compared to the full tangent map $T^m_{\vec{x}_n}$. However, there is a reason to believe that the increase in numerical errors might not necessarily be significant, which follows from the proposition below.

Proposition 3.1 *Let $\widetilde{T}^m_{\vec{x}}$ be the m-step reduced-rank tangent map at $\vec{x}$ from* (3.4) *of rank L. Then, as $m \to \infty$,*

(1) *$\widetilde{T}^m_{\vec{x}}$ spans the L-dimensional tangent subspace at $\vec{x}$ which has either the fastest growing phase volume if L is smaller than the Kaplan-Yorke dimension, or the slowest decaying phase volume if L is larger than the Kaplan-Yorke dimension.*

(2) *$(T^m_{\vec{x}} - \widetilde{T}^m_{\vec{x}})$ spans the $(L+1)$-th Lyapunov subspace at $\vec{x}$.*

Sketch of Proof (1) Observe that, by construction, $\widetilde{Q}_m$ consists of the first L columns of Q_m, while $\widetilde{R}_m$ is the upper-left $L \times L$ segment of R_m. Then, one can show that the volume, spanned by the columns of $\widetilde{T}^m_{\vec{x}}$, is

$$\mathrm{vol}(\widetilde{T}^m_{\vec{x}}) = \prod_{i=1}^{L}\prod_{j=1}^{m}(R_j)_{ii} = \exp\Big(\sum_{i=1}^{L}\sum_{j=1}^{m}\log(R_j)_{ii}\Big). \tag{3.5}$$

In the limit as $m \to \infty$,

$$\sum_{j=1}^{m}\log(R_j)_{ii} \sim m\lambda_i, \tag{3.6}$$

where λ_i is the i-th Lyapunov exponent (see [9]). Therefore, as $m \to \infty$,

$$\mathrm{vol}(\widetilde{T}^m_{\vec{x}}) \sim \mathrm{e}^{(\lambda_1+\cdots+\lambda_L)m}. \tag{3.7}$$

In particular, if L happens to be the Kaplan-Yorke dimension, $\mathrm{vol}(\widetilde{T}^m_{\vec{x}}) \sim \mathrm{const}$.

(2) Let us denote the k-th column of Q_m as $\vec{q}_k$. Observe that the last $(N-L)$ columns of the matrix

$$E_m = Q_0 R_1^{-1} \cdots R_m^{-1}\Lambda_m \tag{3.8}$$

span the $(L+1)$-th Lyapunov subspace as $m \to \infty$ (see [9]), where $\Lambda_m = \mathrm{diag}(R_m, \cdots, R_1)$. In particular, one can show that

$$T^m_{\vec{x}}E_m = Q_m\Lambda_m, \quad \widetilde{T}^m_{\vec{x}}E_m = (\widetilde{Q}_m|0)\Lambda_m, \tag{3.9}$$

where $(\widetilde{Q}_m|0) = (\vec{q}_1, \cdots, \vec{q}_L, 0, \cdots, 0)$ is the $N \times N$ matrix. Then, denoting $\widehat{Q}_m = Q_m - (\widetilde{Q}_m|0)$, we obtain

$$(T^m_{\vec{x}} - \widetilde{T}^m_{\vec{x}})E_m = \widehat{Q}_m\Lambda_m. \tag{3.10}$$

The first L columns of $\widehat{Q}_m\Lambda_m$ are zeros, while the rest decay as $\sim \mathrm{e}^{m\lambda_{L+1}}$.

Remark 3.1 If all Lyapunov exponents starting with λ_{L+1} are negative with large absolute value, an N-dimensional phase volume rapidly becomes L-dimensional under the model dynamics, shrinking along the $(L+1)$-th Lyapunov subspace. Then, if there is a subset $\{\vec{x}\}_{L+1}$ of model variables roughly aligned with $(L+1)$-th Lyapunov subspace on the $\rho_{\vec{F}}$-large part of the model attractor, average errors in $\widetilde{T}^m_{\vec{x}_n}$ for the rest of the model variables (denoted as $\overline{\{\vec{x}\}}_{L+1}$) should not be too significant. Thus, if the response function $A(\vec{x})$ and the columns of the forcing matrix $w(\vec{x})$ are restricted to $\overline{\{\vec{x}\}}_{L+1}$, then the errors in the response produced by $\widetilde{T}^m_{\vec{x}_n}$ are expected to be small.

Below we study the reduced-rank tangent map algorithm, developed above, for two different dynamical systems: the full Lorenz 96 model with time scale separation (see [8, 11, 20]), and the T21 barotropic model on the sphere with realistic Earth topography (see [2, 4, 12, 26]). Although the reduced-rank tangent map strategy is available for an arbitrary small forcing and response function, just as the full-rank tangent map algorithm, here we consider relatively simple types of external forcing and response functions. The models are perturbed by the small constant perturbation, such that $w(\vec{x})$ and $\delta\vec{f}(t)$ in (2.4) are the identity matrix I and constant vector $\delta\vec{f}$, respectively. Additionally, the response function is $A(\vec{x}) = \vec{x}$, which corresponds to the response of the mean state of the model. Under the above assumptions, the linear response is given by

$$\delta_t \rho_{\vec{f}}(\vec{x}) = \mathcal{R}(t)\delta\vec{f}, \quad \mathcal{R}(t) = \lim_{s\to\infty} \frac{1}{s}\int_0^s \mathrm{d}\tau \int_0^t T^r_{\vec{x}(\tau)}\mathrm{d}r. \tag{3.11}$$

Below we are going to study the errors in response produced by the response operator $\widetilde{\mathcal{R}}$, which is obtained via (3.11) from the reduced-rank tangent map $\widetilde{T}$, depending on the rank of $\widetilde{T}$. The errors are determined by comparison with the ideal response operator $\mathcal{R}_I$, which is obtained by perturbing the model and measuring the response directly. For more details on the ideal response operator, see [1–3, 22]. We use the following formula for the relative error estimate:

$$\text{Error} = \Big[\frac{\int_0^{\frac{2}{\lambda_1}} \|\mathcal{R}(t) - \mathcal{R}_I(t)\|^2 \mathrm{d}t}{\int_0^{\frac{2}{\lambda_1}} \|\mathcal{R}_I(t)\|^2 \mathrm{d}t}\Big]^{\frac{1}{2}}, \tag{3.12}$$

i.e., it is the norm $\|\mathcal{R}(t)-\mathcal{R}_I(t)\|$ over twice the e-folding time, divided by the same norm of the ideal response operator $\|\mathcal{R}_I(t)\|$. The time period of integration $\frac{2}{\lambda_1}$, which is twice the e-folding time, is chosen as follows: it was observed before (see [1–3]) that the numerical instability typically manifests itself in $T^t_{\vec{x}}$ at three times the e-folding time. Therefore, the time period of twice the e-folding time is safe enough to obtain clean results without numerical instability.

4 Numerical Experiment 1: the Full Lorenz 96 Model

The full Lorenz 96 (L96) model (see [8, 11, 20]) is given by

$$\begin{aligned} \dot{X}_k &= X_{k-1}(X_{k+1} - X_{k-2}) - X_k + F - \lambda\sum_{j=1}^{J} Y_{k,j}, \\ \dot{Y}_{k,j} &= \frac{1}{\varepsilon}[Y_{k,j+1}(Y_{k,j-1} - Y_{k,j+2}) - Y_{k,j}] + \lambda X_k, \end{aligned} \qquad \varepsilon > 0,\ \lambda > 0, \tag{4.1}$$

where $1 \le k \le K$, $1 \le j \le J$. The following notations are adopted above:

- $\vec{X}$ is a set of "slow" variables of size K. The following periodic boundary conditions hold for $\vec{X}$: $X_{k+K} = X_k$.
- $\vec{Y}$ is a set of "fast" variables of size $K \times J$. The following boundary conditions hold for $\vec{Y}$: $X_{k+K,j} = X_{k,j}$ and $X_{k,j+J} = X_{k+1,j}$.
- F is the external forcing parameter;
- ε is the time scale separation parameter;

- λ is the coupling parameter.

If $J = 0$, then the full Lorenz 96 model in X-variables coincides with the standard Lorenz 96 model (see [20, 21]). The standard Lorenz 96 model in a chaotic regime has the band of linearly unstable wavenumbers, which have westward phase and eastward group velocities, just like actual Rossby waves in the atmosphere. The Y-variables play the role of small scale fast unresolved interactions, common in the large-scale geophysical models. Note that the Y-variables do not have the forcing term F, while possessing the same linear damping term as X-variables, thus being strongly dissipative. For the full Lorenz 96 model, one can expect the reduced-rank tangent map of rank $L \geq K$ to perform well for the subset of X-variables. We perform the direct numerical simulations with the full Lorenz 96 model for the following numerical parameters:

- Number of degrees of freedom $K = 8, 12, 18$, $J = 8, 5, 3$ (so that the total number of variables in each case is 72);
- 4th-order Runge-Kutta time integrator;
- Numerical time step $\Delta t = 0.005$;
- Value of constant forcing $F = 8$;
- Value of the time scale separation parameter $\varepsilon = 0.1$;
- Value of the coupling parameter $\lambda = 0.1$.

The Lyapunov exponents of the full Lorenz 96 model for the regime with forcing $F = 8$ and the dimensions $K = 8, 12, 18$, $J = 8, 5, 3$ are shown in Figure 1, while the dynamical properties associated with Lyapunov exponents, such as the Kolmogorov-Sinai entropy and the Kaplan-Yorke dimension, are displayed in Table 1. Observe that, for the full Lorenz 96 model and

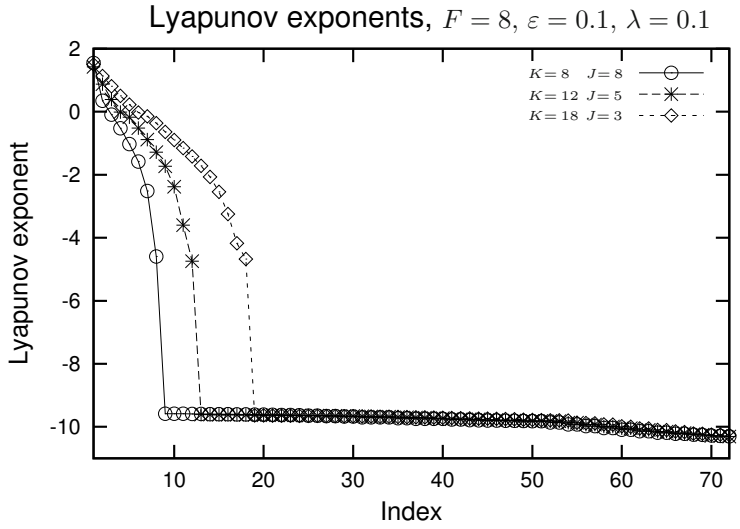

Figure 1 Lyapunov exponents for the full Lorenz 96 model, $F = 8$, $\varepsilon = 0.1$, $\lambda = 0.1$. Dimensions: $(K = 8, J = 8)$, $(K = 12, J = 5)$, $(K = 18, J = 3)$.

Table 1 Properties of Lyapunov exponents for full Lorenz 96 model, $F = 8$, $\varepsilon = 0.1$, $\lambda = 0.1$. Dimensions: $(K = 8, J = 8)$, $(K = 12, J = 5)$, $(K = 18, J = 3)$. Notations: λ_1 — largest Lyapunov exponent; N_{pos} — number of positive Lyapunov exponents; "KS-ent." — Kolmogorov-Sinai entropy; "KY-dim." — Kaplan-Yorke dimension.

Properties of Lyapunov exponents Full L96, $F = 8$, $\varepsilon = 0.1$, $\lambda = 0.1$				
	λ_1	N_{pos}	KS-ent.	KY-dim.
$K = 8$, $J = 8$	1.55	2	1.897	5.158
$K = 12$, $J = 5$	1.427	3	2.689	7.86
$K = 18$, $J = 3$	1.498	5	4.168	11.66

observed regimes, there is a distinct separation in the Lyapunov exponent spectrum. Namely, the first K Lyapunov exponents exhibit "typical" behavior, displaying gradual decay with increasing index, while the last JK Lyapunov exponents all have values of around -10, which means that the phase volume of the $(K + 1)$-th Lyapunov subspace shrinks extremely rapidly

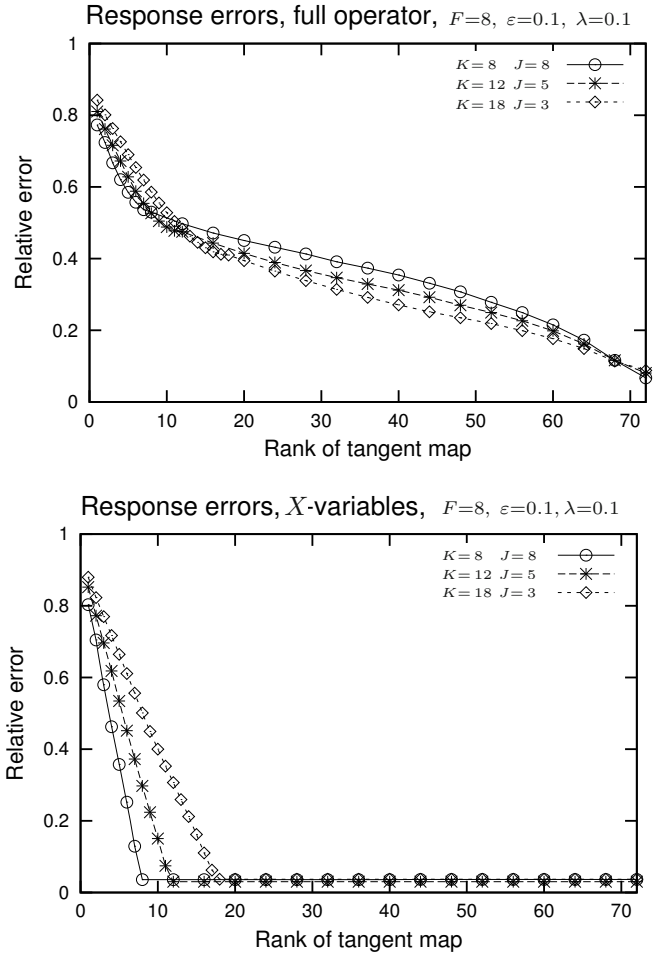

Figure 2 Response errors of different rank tangent maps for the full Lorenz 96 model, $F = 8$, $\varepsilon = 0.1$, $\lambda = 0.1$. Dimensions: $(K = 8, J = 8)$, $(K = 12, J = 5)$, $(K = 18, J = 3)$. Left picture — errors of full response operators. Right picture — errors of the response operators at X-variables.

in all regimes. Clearly, the $(K+1)$-th Lyapunov subspace in each regime is associated with the small scale Y-variables, which do not have forcing terms. The relative errors between the actual "ideal" response and the linear response operators for tangent map with different ranks, computed according to the formula (3.12), are shown in Figure 2. As we can see, the reduction of the rank of the tangent map for the full response operator (which includes both X and Y variables in both forcing and response) causes gradual growth of the error between the linear response and the actual "ideal" response. However, the same reduction of the rank of the tangent map for the response operator, restricted to the X-variables in both response and forcing, has no effect on the response error (which does not exceed 2%), for the response computed with the tangent map of any reduced rank $\geq K$. Remarkably, the response computed with the tangent map of rank $\geq K$ has the same precision as the response computed with the full rank tangent map, which is predicted in Remark 3.1. When the rank of the tangent map becomes less than K, linear growth of the response error is observed. This is true for all regimes of the full Lorenz 96 model studied here.

5 Numerical Experiment 2: the T21 Barotropic Truncation

The model equations for the T21 barotropic truncation on a sphere are

$$\begin{aligned} &\frac{\partial \zeta}{\partial t} + \nabla^{\perp}\psi \cdot q = \Big(-\frac{1}{\tau} + K\Delta^3\Big)\zeta + \zeta^*, \\ &\zeta = \Delta\psi, \quad q = \zeta + 2\Omega \sin\theta\Big(1 + \frac{h}{H}\Big). \end{aligned} \tag{5.1}$$

The physical units for the model length and time are meters and days, respectively. The model variables are the following: ϕ, θ and t are the longitudinal, latitudinal and time coordinates, respectively, $\psi = \psi(\phi, \theta, t)$ is the streamfunction, $\zeta = \zeta(\phi, \theta, t) = \Delta\psi$ is the relative vorticity, $q = q(\phi, \theta, t)$ is the potential vorticity, and $h = h(\phi, \theta)$ is the realistic Earth topography, scaled by the height of the troposphere ($H = 10000$ meters). The physical parameters are the following: $\tau = 15$ days is the Ekman friction time scale, $\Omega = 2\pi$ radian/day is the angular velocity of Earth's rotation, and the scale-selective damping coefficient $K = 3.38 \cdot 10^{-9}$ meter^6/day is chosen so that the damping time scale for the wavenumber 21 is 3 hours.

The function $\zeta^* = \zeta^*(\phi, \theta)$ is the time-independent forcing, which is chosen to roughly match the properties of model climatology with observations. In this work, two different types of steady forcing are used in the barotropic model to mimic a realistic climatology at 500 hPa (see [26]) and 300 hPa (see [12]) heights in the troposphere. Furthermore, these two regimes are referred to as Selten and Franzke regimes, respectively.

The model equations in (5.1) are projected onto the triangle-shaped array of spherical harmonics with maximum wavenumber 21 (standard T21 barotropic truncation). The T21 truncation is further restricted to the Northern hemisphere with no flow across the equator. Therefore, the truncated flow is completely described by 231 spectral coefficients. The standard fourth-order Runge-Kutta method is used to integrate the model in time with the time step of 3 hours.

The T21 barotropic model in both Selten and Franzke regimes has been used in [2] to predict the linear response of both mean and variance of the first four empirical orthogonal functions (EOFs). Since, by construction, the EOFs project onto directions of the largest variance in

the model, one can expect that higher EOFs have a tendency to project onto higher Lyapunov subspaces, which, according to Remark 3.1, could result in improved precision of the reduced-rank tangent map algorithm for lower ranks of the tangent map and first few EOFs with largest variance. Here we run the T21 model with the following numerical parameters:

- Number of degrees of freedom 231;
- 4th-order Runge-Kutta time integrator;
- Numerical time step $\Delta t = 3$ hours;
- Two dynamical regimes: Selten regime (mimics the behavior of the atmosphere at 500 hPa height), and Franzke regime (mimics the behavior of the atmosphere at 300 hPa height);
- Both the linear response operator and the actual "ideal" response operator are restricted to the first four EOFs, in both forcing and response.

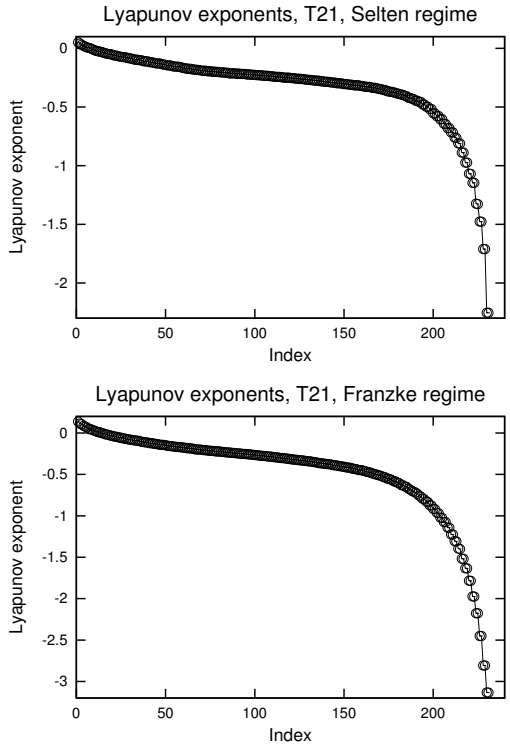

Figure 3 Lyapunov exponents for the T21 model barotropic model, Selten and Franzke regimes.

Table 2 Properties of Lyapunov exponents for T21 model, Selten and Franzke regimes. Notations: λ_1 — largest Lyapunov exponent; N_{pos} — number of positive Lyapunov exponents; "KS-ent." — Kolmogorov-Sinai entropy; "KY-dim." — Kaplan-Yorke dimension.

Properties of Lyapunov exponents, T21 model				
	λ_1	N_{pos}	KS-ent.	KY-dim.
Selten regime	$5.071 \cdot 10^{-2}$	7	0.1662	15.05
Franzke regime	0.1373	14	0.7878	30.75

The Lyapunov exponents of the T21 model for both the Selten and Franzke regimes are shown in Figure 3, while the dynamical properties associated with Lyapunov exponents, such as the Kolmogorov-Sinai entropy and Kaplan-Yorke dimension, are displayed in Table 2. Observe that there is no separation in the spectrum of Lyapunov exponents for both Selten and Franzke regimes, which initially suggests that the reduced tangent map algorithm would not be too successful. However, the relative errors between the actual "ideal" response and the linear response operators for tangent map with different ranks, computed according to the formula (3.12) and shown in Figure 4, indicate that there is sharp decrease of the response error when the rank of the tangent map is increased (for relatively small ranks of the tangent map), for both Selten and Franzke regimes, in particular, the relative error is already about 10% when the tangent map has rank 50 (less then one quarter of the total number of variables, 231). These results suggest that the EOF coordinate system has the advantage over the generic model coordinate system, as it may roughly align the model coordinates with Lyapunov subspaces on ρ-large parts of the model attractor.

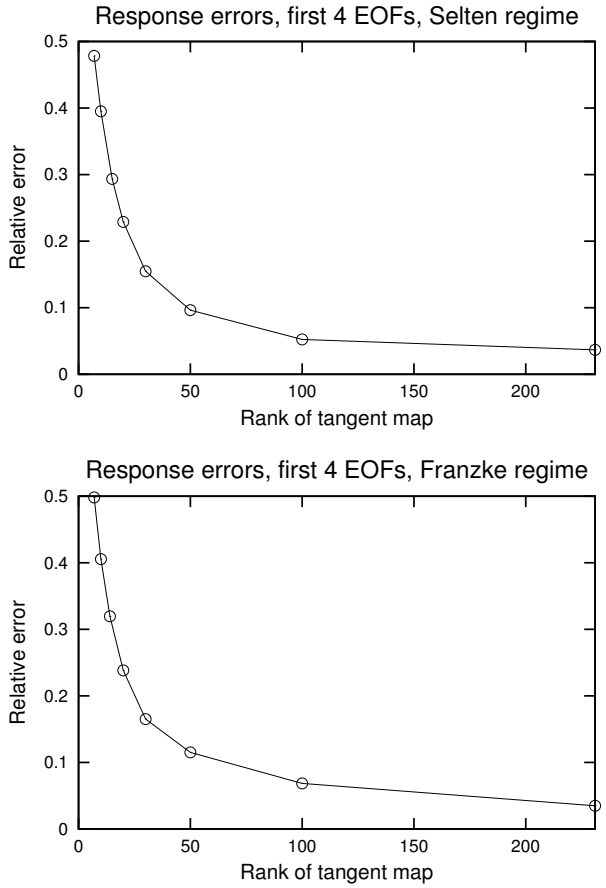

Figure 4 Response errors of different rank tangent maps for the T21 model barotropic model, Selten and Franzke regimes.

6 Conclusions

In this work, we propose a numerical algorithm for the short-time linear response formula (see [1–3]) which can significantly reduce computational cost at the expense of slightly increased response errors. The algorithm is based on the reduced-rank tangent map of rank L (with $L \leq N$, N being the total number of model variables). This reduced-rank tangent map is computed in such a way that it spans the L-dimensional tangent subspace which has the fastest growing/slowest decaying phase volume, while the difference between the full rank and reduced-rank tangent map spans the $(L+1)$-th Lyapunov subspace. Due to these properties, in the case when all Lyapunov exponents corresponding to the $(L+1)$-th Lyapunov subspace are negative with large absolute value, and there is a subset of model variables associated with this subspace, the errors in the linear response formula for the rest of the variables produced by the reduced-rank tangent map are expected to be small. Here we study the new algorithm for two different models: the full Lorenz 96 model and the T21 barotropic truncation with realistic topography. The results are summarized below.

The full Lorenz 96 model The full Lorenz 96 model in the studied regimes has a distinct subset of small scale variables which are strongly dissipative. As a result, the Lyapunov subspace of corresponding dimension seems to be roughly aligned with the subset of strongly dissipative small scale variables of the full Lorenz 96 model with strong separation in the spectrum of the Lyapunov exponents, and the linear response on the rest of the variables (the large scale forced variables) is predicted very well by the reduced tangent map as long its rank is equal to or exceeds the dimension of the subset of large scale forced variables. In fact, there is no difference in relative error (which is about 2%) between the linear responses with full rank and reduced-rank tangent maps. By contrast, the reduced-rank tangent map algorithm does not perform well for the full linear response operator, which includes both large scale forced variables and small scale dissipative variables (the error starts growing immediately as the rank of the tangent map is reduced).

The T21 barotropic truncation The T21 barotropic truncation with realistic topography is tested in two dynamical regimes, corresponding to the dynamics of the atmospheric airflow at 300 hPa and 500 hPa geopotential height. The subset of model variables for linear response corresponds to the first four empirical orthogonal functions (EOFs). Due to the fact that first EOFs span the subspace with largest total variance in the corresponding dimension, it is likely that the complementary subspace, consisting of higher-order EOFs, is frequently aligned with the corresponding Lyapunov subspace on the attractor. As a result, the remarkable reduction of response errors is observed as the rank of the tangent map is increased even for relatively small ranks: in fact, for the reduced-rank tangent map with rank 50 (less than one quarter of the total number of variables, 231), the relative error in the linear response is already about 10%. This trend is observed for both the 300 hPa and 500 hPa dynamical regimes, none of which has separation in the Lyapunov exponent spectrum.

Overall, the results of this study confirm the usability of the reduced-rank tangent map algorithm for special situations, where the linear response to be predicted is restricted to the large scale variables with rich dynamics and weak dissipation. However, this special situation seems to be relatively frequent in geophysical models with main large scale model variables

being complemented by the small scale "unresolved" variables. If the linear response in such a model is restricted to the large scale variables in both forcing and response, and the small scale variables are dissipative (or, at least, not strongly forced), the new reduced-rank linear response algorithm may produce results of comparable precision at substantially decreased computational cost.

Acknowledgement The author thanks Professor Andrew Majda for pointing him towards the full Lorenz 96 model with time scale separation, which made a perfect example of the situation where the reduced-rank tangent map algorithm is as efficient as the full rank tangent map algorithm.

References

[1] Abramov, R. and Majda, A., Blended response algorithms for linear fluctuation-dissipation for complex nonlinear dynamical systems, *Nonlinearity*, **20**, 2007, 2793–2821.

[2] Abramov, R. and Majda, A., A new algorithm for low-frequency climate response, *J. Atmos. Sci.*, **66**(2), 2009, 286–309.

[3] Abramov, R. and Majda, A., New approximations and tests of linear fluctuation-response for chaotic nonlinear forced-dissipative dynamical systems, *J. Nonlinear Sci.*, **18**(3), 2008, 303–341.

[4] Abramov, R., Majda, A. and Kleeman, R., Information theory and predictability for low frequency variability, *J. Atmos. Sci.*, **62**(1), 2005, 65–87.

[5] Bell, T., Climate sensitivity from fluctuation dissipation: Some simple model tests, *J. Atmos. Sci.*, **37**(8), 1980, 1700–1708.

[6] Carnevale, G., Falcioni, M., Isola, S., et al, Fluctuation-response in systems with chaotic behavior, *Phys. Fluids A*, **3**(9), 1991, 2247–2254.

[7] Cohen, B. and Craig, G., The response time of a convective cloud ensemble to a change in forcing, *Quart. J. Roy. Met. Soc.*, **130**(598), 2004, 933–944.

[8] Crommelin, D. and Vanden-Eijnden, E., Subgrid scale parameterization with conditional Markov chains, *J. Atmos. Sci.*, **65**(8), 2008, 2661–2675.

[9] Eckmann, J. and Ruelle, D., Ergodic theory of chaos and strange attractors, *Rev. Mod. Phys.*, **57**(3), 1985, 617–656.

[10] Evans, D. and Morriss, G., Statistical Mechanics of Nonequilibrium Liquids, Academic Press, New York, 1990.

[11] Fatkullin, I. and Vanden-Eijnden, E., A computational strategy for multiscale systems with applications to Lorenz 96 model, *J. Comput. Phys.*, **200**(2), 2004, 605–638.

[12] Franzke, C., Dynamics of low-frequency variability: Barotropic mode, *J. Atmos. Sci.*, **59**(20), 2002, 2897–2909.

[13] Gritsun, A., Fluctuation-dissipation theorem on attractors of atmospheric models, *Russ. J. Numer. Math. Modeling*, **16**(2), 2001, 115–133.

[14] Gritsun, A. and Branstator, G., Climate response using a three-dimensional operator based on the fluctuation-dissipation theorem, *J. Atmos. Sci.*, **64**(7), 2007, 2558–2575.

[15] Gritsun, A., Branstator, G. and Dymnikov, V., Construction of the linear response operator of an atmospheric general circulation model to small external forcing, *Num. Anal. Math. Modeling*, **17**, 2002, 399–416.

[16] Gritsun, A., Branstator, G. and Majda, A., Climate response of linear and quadratic functionals using the fluctuation dissipation theorem, *J. Atmos. Sci.*, **65**(9), 2008, 2824–2841.

[17] Gritsun, A. and Dymnikov, V., Barotropic atmosphere response to small external actions: theory and numerical experiments, *Atmos. Ocean Phys.*, **35**(5), 1999, 511–525.

[18] Kubo, R., Toda, M. and Hashitsume, N., Statistical Physics II: Nonequilibrium Statistical Mechanics, Springer-Verlag, New York, 1985.

[19] Leith, C., Climate response and fluctuation-dissipation, *J. Atmos. Sci.*, **32**(10), 1975, 2022–2026.

[20] Lorenz, E., Predictability: a problem partly solved, Proceedings of the Seminar on Predictability, European Centre for Medium-Range Weather Forecast, Shinfield Park, Reading, England, 1996.

[21] Lorenz, E. and Emanuel, K., Optimal sites for supplementary weather observations, *J. Atmos. Sci.*, **55**(3), 1998, 399–414.

[22] Majda, A., Abramov, R. and Grote, M., Information Theory and Stochastics for Multiscale Nonlinear Systems, CRM Monograph Series, **25**, A. M. S., Providence, RI, 2005.

[23] Risken, F., The Fokker-Planck Equation, Second Edition, Springer-Verlag, New York, 1988.

[24] Ruelle, D., Differentiation of SRB states, *Comm. Math. Phys.*, **187**(1), 1997, 227–241.

[25] Ruelle, D., General linear response formula in statistical mechanics, and the fluctuation-dissipation theorem far from equilibrium, *Phys. Lett. A*, **245**(3–4), 1998, 220–224.

[26] Selten, F., An efficient description of the dynamics of barotropic flow, *J. Atmos. Sci.*, **52**(7), 1995, 915–936.

[27] Young, L.-S., What are SRB measures, and which dynamical systems have them? *J. Stat. Phys.*, **108**(5–6), 2002, 733–754.